JOURNAL OF CATALYSIS 113, 281–294 (1988)

Co/Mo/Alumina Catalyst Structure Determination by EXAFS

IV. Co–K Edge in the Oxide and Sulfided States

N.-S. CHIU, M. F. L. JOHNSON,[1] AND S. H. BAUER[2]

Department of Chemistry, Baker Laboratory, Cornell University, Ithaca, New York 14853

Received June 13, 1987; revised April 11, 1988

The graded series of Co/Mo/alumina hydrodesulfurization catalysts, which was previously investigated via EXAFS spectroscopy at the Mo–K edge, was further examined at the Co–K edge, both in the initially prepared oxide states and after extended testing in an HDS reactor. The spectra of various Co/S and Co/O reference compounds were recorded concurrently. From the near-edge profiles we obtained estimates of Co(II)/Co(III) ratios, while information on the configuration of O, S, and Co atoms around the Co species was derived from radial distribution functions. The present spectra clearly show that even after extended use in an HDS reactor, a significant fraction of oxide bonds remain. When Co loading is high the Co_9S_8 phase appears. The augmenting effect of the Co promoter is not discernible from the available structural data. However, an empirical correlation, based on the supposition that the enhancement per Co declines smoothly with increased loading, leads to good correspondence between the observed rate constants and those predicted.

INTRODUCTION

The structural model presented in our previous reports (*1, 2*) was derived from analyses of near- and extended-fine structure spectra at the Mo–K edges of a graduated series of Mo/Co/alumina preparations, in the oxide state, after H_2S/H_2 sulfiding, and after extended HDS treatment in a pilot scale reactor. We found direct evidence for small platelets of the catalytically active material distributed over the support surface (*3*). Their composition is somewhat ambiguously represented by O_x–Mo–S_y/Co, indicating incomplete sulfiding even after extended use in the HDS reactor. Structurally, there appears to be a higher regularity in the sulfided states than in the initially calcined oxides, which are clearly amorphous. A nearly linear (but imperfect) correlation was found (*4*) between the measured (activity/unit area) and the number of Mo–S pairs present at the peripheries of the platelets (derived from EXAFS radial distribution functions) per 100 g of catalyst/unit area. The derived ratios of (Mo–Mo)/(Mo–S) for various Co loadings and processing conditions indicated that under extended treatment with sulfur-bearing fuels the cobalt promoter, initially randomly distributed throughout the platelets, diffused to the peripheries and thus anchored the active sites.

A more detailed model of HDS catalyst structure, proposed by Topsøe *et al.* (*5*), was derived by supplementing EXAFS data with results from Mössbauer emission spectra (MES), infrared absorptions of adsorbed gases which served as probes for specific sites, and other techniques. These studies indicated that the cobalt promoter could be present in three distinct forms, although not necessarily concurrently in the same preparation. MES showed that Co participated in MoS_2-type layered structures, but with the cobalt at edge positions of platelets. When Co loading was high, Co_9S_8 was generated, clearly demonstrated by

[1] Present address: 1124 Elder Road, Homewood, IL 60430.

[2] To whom correspondence should be addressed.

0021-9517/88 $3.00

EXAFS (see below). Some Co may remain in the bulk alumina, to an extent which depends on the temperature and levels of exposure to sulfur-bearing species. Improved EXAFS data reduction procedures (*6*) led us to a model which had few if any MoS_2 crystallites; rather, there were substantial levels of incompletely sulfided, highly distorted MoO_xS_y in rafts, and the metal atoms were in octahedral centers except for those at the peripheries of the platelets. Semiquantitative deductions, based on ratios of peak areas of (Mo–Mo) vs (Mo–S) in the radial distribution curves, indicated that the platelets were small, and incorporated (15 → 50) metal–metal scattering pairs.

In this report we present structural information for the same group of preparations, derived from near- and extended-fine structure X-ray absorption spectra recorded in the vicinity of the Co–K edge. We were looking for (i) a proper description of the O/S environments around the Co atoms, (ii) measures of the Co(III)/Co(II) ratios present in the oxide and sulfided states, (iii) confirmation that the sulfiding process was only partial, (iv) an indication that the Co atoms tended to segregate to the peripheries of the platelets upon extended use in an HDS reactor, and (v) some structural feature associated with Co that would reproduce the observed correlations with activity to a higher degree than was reported in the preceding communication (*3*). With these we were only partially successful; the X-ray absorption spectra at the Co–K edge were considerably more noisy than those at the Mo–K edge, and the deduced radial distribution curves had lower resolution.

EXPERIMENTAL

The $Co/Mo/Al_2O_3$ catalysts were prepared as described in our previous report (*3*). The compositions of our samples varied over 6–30% in MoO_3 (nominally, 6, 12, 18, 24, 30%) and 1.5–12% in CoO (1.5, 3, 6, 12%). The reference structures for EXAFS analyses at the Co–K edge (oxides) were $Co(AcAc)_3$, furnished by Professor L. Que (*7*); $CoMoO_4$ from ARCO Technical Center; Co_3O_4 from the Melton Chemical Co.; $CoCO_3$, $Co(OH)_2$, and $Co(NO_3)_2 \cdot 6H_2O$ were available at Cornell. Reference compounds for the sulfided states were Co_9S_8 (ARCO) and $Co(S_2CN\varepsilon t_2)_3$ (Prof. Que). All these materials were used without further purification.

The EXAFS experiments were performed at the Cornell High Energy Synchrotron Source. Due to the high absorption by Mo at the Co–K edge (7.709 kV), and crystal "glitches" (*8*) with the channel-cut silicon crystals using symmetric 220 and 111 reflection planes, the samples with low Co and high Mo gave unacceptable transmission data. Hence all our structural conclusions are based on fluorescence scans, and thus we maintained a consistent diagnostic in our search for structural trends with composition. However, for many samples both transmission and fluorescence data were collected to establish calibrations; the transmission data were used for reference purposes only. A scintillation counter and filter-assembled ion chamber (*9*) were used to record the fluorescence spectra. Transmission experiments were performed with a conventional configuration using an Ar-filled ion chamber for the detector. For both modes of operation beam intensities were monitored with a N_2-filled chamber. The disadvantage of relying solely on fluorescence spectra is that they are considerably more noisy than transmission runs, even when one uses a good detector system, such as an ion chamber. The spectrum of a light element, as a minor constituent in the presence of a heavier absorber, is unavoidably noisy. We used autocorrelation smoothing (*10*), which has the advantage that it is more effective than a running average (*11*), without cutting off too many data points at the ends of the spectra. However, the useful records for the low Co concentration samples were limited to about 500 eV beyond the Co–K edge.

For each spectral scan two reductions

were performed. In one, all the available data were retained in spite of the large noise at high k, so as to achieve the best resolution in the *RD* curves. In the second analysis, the spectra were terminated at about 10–12 $Å^{-1}$, to minimize the appearance of spurious peaks and thus provide more reliable comparisons between different samples. For either case, in the first stage of the analysis the background peak (0–1 Å range) in the Fourier transforms was large. This could affect the position of the first peak by as much as 5%, and possibly also shift the peak positions in the second coordination shell. Use of a high-order (third or fourth degree) polynominal, or division of the spectrum into more sections for generating a spline-fit for the background, did eliminate most of the 0- to 1-Å peak but also greatly reduced the detection of small persistent (valid) features in the *RD* spectra (for $2 < R < 3$ Å); 10–20% shift in the peak positions was also introduced. Hence, for most of the analyses we kept the order of the background polynomial and the number of segments as low as possible. In some cases we had to incorporate part of the 0- to 1-Å peak into the first shell peak; therefore we estimate that the first shell area may have an error as high as 20%.

NEAR-EDGE PROFILES

The near-edge profiles for both the oxide preparations and the sulfided catalysts (test reactor) reflect the electronic states and the densities of unoccupied orbitals at the various Co sites. Since the energy dependence of fluorescence features and their intensities are quite reproducible, subtleties in the not-fully-resolved features were made more transparent by computing the corresponding derivatives ($d\mu/dE$). This treatment is a refinement of the procedure we followed in our previous reports wherein we resolved the near-edge absorption functions into overlapping Gaussians. The relation between a recorded pattern and its derivative is illustrated in Fig. 1a for Co (metal); for calibration the energies of all features for the catalyst were measured relative to the sharp first maximum of the metal, set at zero.

The $d\mu/dE$ functions may be interpreted in two ways: (i) as empirical fingerprints, by comparing unknown with known spectra, relative to shapes and energy locations; (ii) by assigning specific state-to-state designations to each feature, thus deducing the location of the upper energy states relative to the 1s core state.

Careful inspection of the derivative functions leads to the following empirical conclusions. The XANES spectra of four reference compounds [$CoCO_3$; $Co(OH)_2 \cdot 2H_2O$; $Co(NO_3)_2 \cdot 6H_2O$; and β-$CoMoO_4$] are qualitatively indistinguishable; Fig. 1b shows the spectrum of one of these, β-$CoMoO_4$. In these compounds Co^{2+} is surrounded by distorted octahedra of oxygen atoms. The intense relatively narrow peaks (which correspond to smooth, sharply rising absorption feature) appear within ±0.6 eV of their mean, but the small third maximum wanders (23 vs 29 eV); however, its shape is maintained. The location of the major peak in Co^{3+} $(AcAc)_3$, shown in Fig. 1c, is shifted by approximately 3 eV to higher energies, as expected for the higher oxidation state (*12*). The pattern for Co_3O_4, Fig. 1d, clearly indicates mixed oxidation states (Co^{2+} in distorted tetrahedral sites; Co^{3+} in octahedral sites, in the ratio 1/2).

The profiles of the catalyst preparations in the oxide state show a trend consistent with Co loading, with a minor dependence on the Mo content. The principal peak is broad, being a superposition of two peaks (approximately at 9 and 12 eV) as in Co_3O_4, but their relative intensity switches (i.e., 12 rises; 9 falls) with increasing Mo content. However, the peak at 17.8 eV of Co_3O_4 does not develop even as a significant shoulder. The patterns Mo/Co = 30/1.5 and 30/3 (Fig. 1e) are similar to $CoMoO_4$ but shifted by ≈2 eV to higher energies. When the atomic ratio (Co/Mo) > 1 an obvious shoulder appears at ≈17 eV, which be-

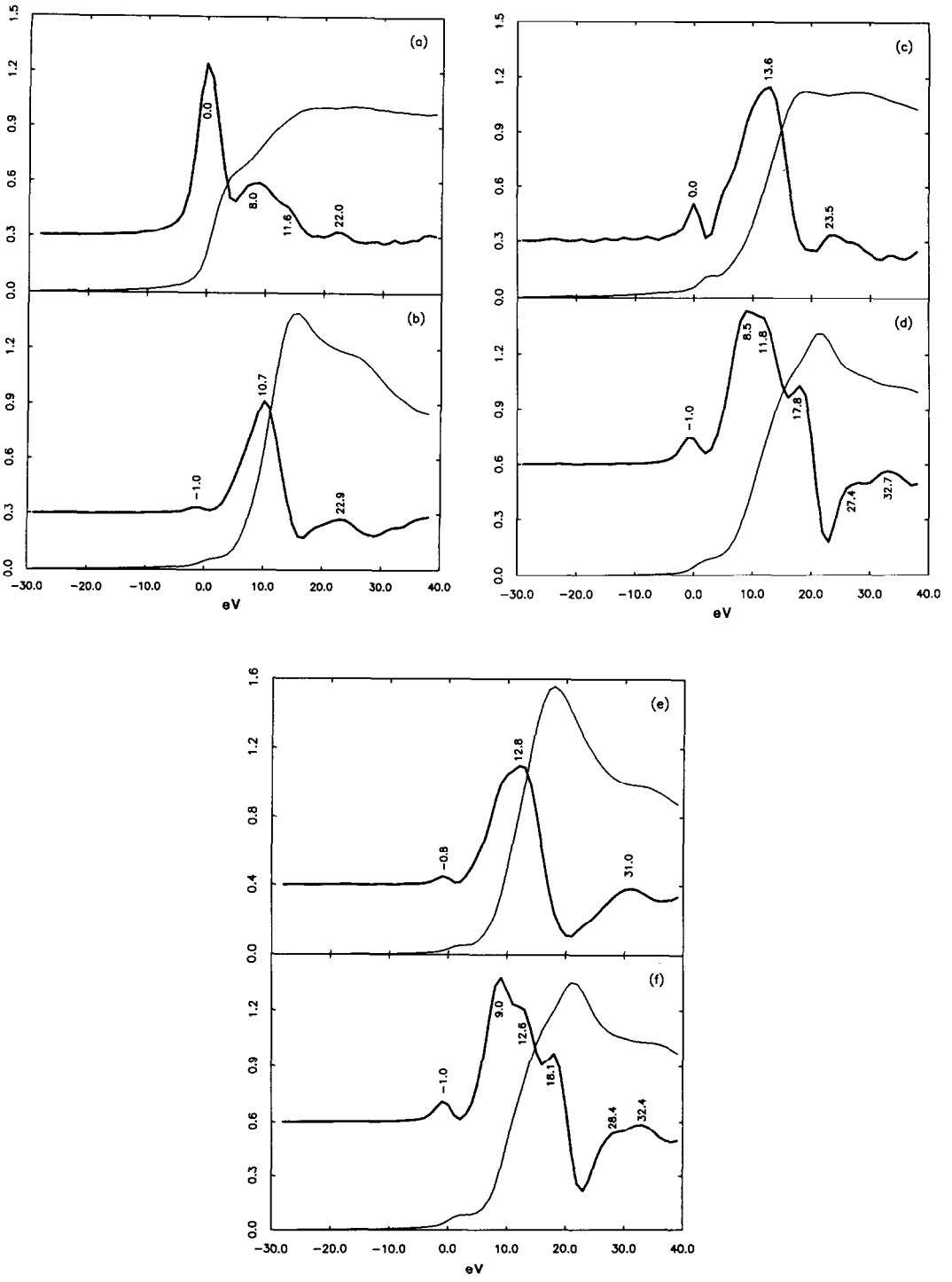

FIG. 1. Near-edge profiles (and derivatives) at the Co–K edge of reference compounds and the catalyst preparations (oxide state); fluorescence records: (a) Co (metal), (b) β-$CoMoO_4$, (c) Co $(AcAc)_3$, (d) Co_3O_4, (e) Mo/Co = 30/3, (f) Mo/Co = 12/12. Note similarity in shape but displaced location of catalysts relative to β-$CoMoO_4$.

comes increasingly more prominent; eventually the pattern approaches that of Co_3O_4 (Fig. 1f). While these XANES profiles show that even at the high Co loading, clear-cut Co_3O_4 structural units are not fully developed, a useful description is to consider the oxides as Co^{2+} residing within a mix of distorted tetrahedra and octahedra of oxygens, with increasing proportions of Co^{3+} located in the octahedra for the higher cobalt loadings. The possible mixing of Co and Mo species within the sea of oxygen atoms cannot be discerned from these data.

Only two reference compounds were available for the sulfided states, Co^{3+} 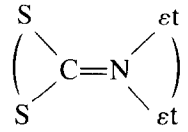 and $Co_9^{2+}S_8$. Their derivative functions are plotted in Figs. 2a and 2b. While they clearly have distinctive profiles, note that the principal peaks [i.e., the location of maximum slopes in their $\mu(E)$ functions] are similar: 4.6 eV for Co_9S_8; 5.5 eV for the thio compound.

Except for two catalysts that are heavily loaded with cobalt (Mo/Co, nominal weight percent 12/12 and 18/12), the XANES profiles of the sulfided catalysts resemble more closely those of the oxide preparations than they do the reference sulfides. A typical derivative curve of the group (6/1.5; 6/3; 12/1.5; and 12/3) is illustrated in Fig. 2c. The principal peak is a closely spaced superposition of two transitions. Samples with composition (18/1.5 and 30/1.5) have the same profile but with a wider separation between the overlapping transitions. Comparison with Fig. 1 patterns shows that these are similar, both in shape and in location, to the XANES of the oxides (range from 6/3 to 18/3). We consider this strong evidence for incomplete sulfiding of the cobalt oxides (particularly of preparations

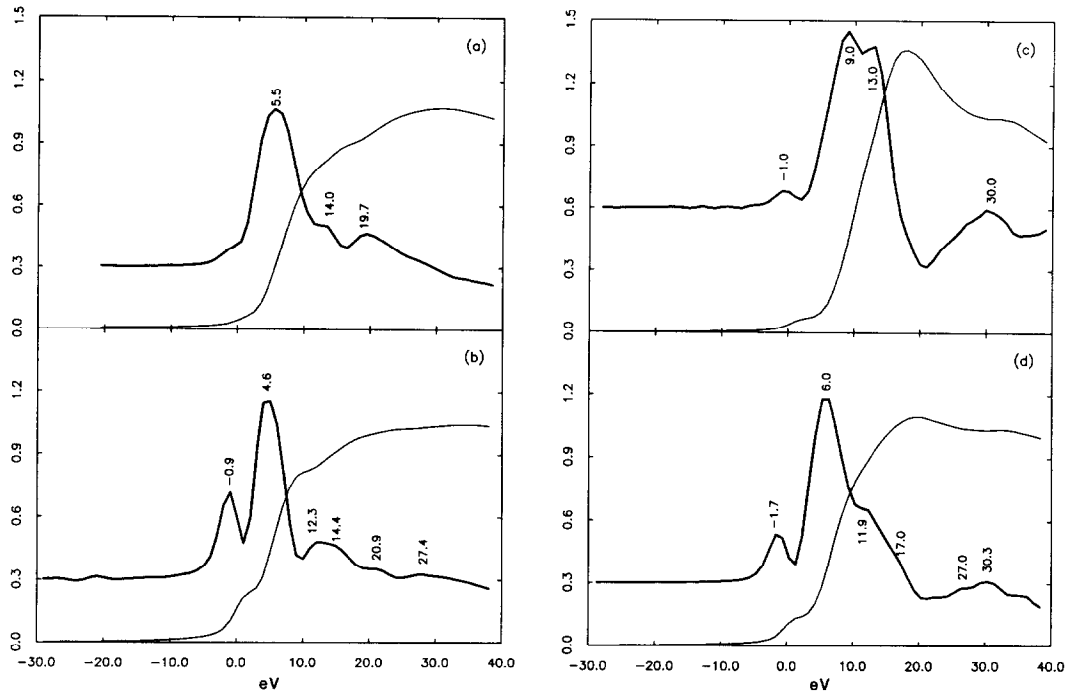

FIG. 2. Near-edge profiles (and derivatives) of reference compounds and selected sulfided catalysts: (a) Co 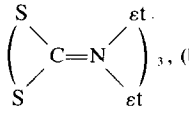 , (b) Co_9S_8, (c) Mo/Co = 12/1.5, (d) Mo/Co = 12/12.

with low cobalt content) even after extensive treatment with sulfur-bearing organic species, under typical reactor conditions. The four preparations (18/3; 6/6; 12/6; and 30/6) show a trend toward Co_9S_8, but are still dominated by the patterns of the residual oxides. Finally, the two preparations (12/12 and 18/12; Fig. 2d) do resemble Co_9S_8, but still have a considerable oxide component. Thus, as we demonstrated via their EXAFS spectra at the molybdenum–K edge (*2*), sulfiding of the oxides is not complete; and the catalytic moiety should be designated an oxysulfide.

The assignment of spectroscopic transitions at the K edges for the 3*d* transition metal oxides is problematic (*12*). It has been established that the one-electron formulation accounts satisfactorily for the near-edge profiles of the metals. Because in good conductors the core-hole is effectively screened, calculations based on neglect of the core-hole appear adequate. Then the edge absorption profile is primarily sensitive to the electron density near the Fermi level. Atomic type selection rules generally apply. The best calculations (*13*) include both the initial state and the final state broadening effects.

In the oxides, the location of the edge (defined as the energy of a point half-way up to the absorption maximum) is shifted to higher values due to lowering of the 1*s* core levels (*14*). Because the oxides are insulators, the core hole is incompletely screened, so that many-body effects become involved. No quantitative agreement between experiment and calculations has been achieved. A generally accepted analysis is based on a molecular orbital description for a metal ion residing within a coordination shell of oxygens, in an octahedral (regular or distorted) or tetrahedral configuration. Dipole selection rules are applied (*15*).

The three distinct features (Fig. 1) are typical of these metal oxide spectra. The first is a weak quadrupole excitation from 1*s* to $2t_{2g}$ and $3e_g$ (mostly 3*d* in character). These are stronger in tetrahedrally coordinated configurations (or highly distorted octahedra) than in symmetric octahedra. The second has been assigned to $1s \rightarrow 3a_{1g}$ (mostly 4*s*), but this has been questioned. The most intense absorption is identified as $1s \rightarrow 4t_{1u}$ (mostly 4*p*). Asymmetric metal–ligand bonding leads to splitting of the degenerate antibonding orbitals. This causes broadening of the spectral features (*16*).

From the preceding discussion it is clear that the profiles recorded for these catalysts (and of the reference compounds) follow the general patterns previously reported for 3*d* transition metal oxides. The objective of this investigation was to ascertain whether *small differences* in profiles correlate with Co/Mo content and associated catalytic activity. It appears that except for the heavily loaded samples the differences observed were essentially within the random fluctuations of this type of spectroscopy.

EXAFS and Radial Distributions (Oxides)

In the oxide state, the radial distribution functions for atomic ratio Co/Mo < 1 preparations are similar, as illustrated in Figs 4a–4c [in our designation (*11, 12*), we show $\rho_3(R\psi)$, prior to phase-shift correction], somewhat like β-$CoMoO_4$ (Fig. 3b). All show a strong peak at 1.9–2.0 Å, and a small peak at 3.35–3.45 Å (phase-shift corrected). Consistently, a smaller feature that is not due to noise appears at ≈2.8 Å, but with variable intensity. The major peak is clearly due to Co–O scattering, as observed in $Co(AcAc)_3$ (Fig. 3c). The peak at ≈3.4 Å may be assigned to an overlap of Co(t)–Co(t) and Co(o)–Co(o), as found in Co_3O_4, Fig. 3a. (The *o* and *t* in parentheses indicate octahedral and tetrahedral sites, respectively.) The position of the first peak moves to lower *R* with increasing Co content. In Co_3O_4 the unresolved octahedral Co(o)–O (1.89 Å, about 80%) and tetrahedral Co(t)–O (1.99 Å, about 20%) generate a single peak at 1.92 Å; the Co–O in $CoMoO_4$ is located at 2.04 Å, and we estimate that Co–O in CoO is 2.1 Å. Hence in the cata-

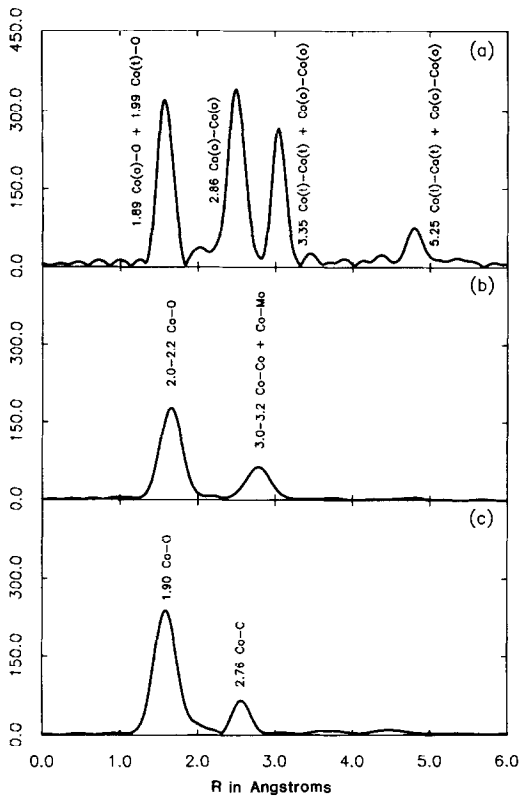

FIG. 3. $\rho_3(R\psi)$ curves of oxide preparations and of reference compounds. (a) Co_3O_4, EXAFS data extended to k = 15 Å^{-1}; (b) β-$CoMoO_4$, EXAFS data terminated at k = 12 Å^{-1}; (c) $Co(AcAc)_3$.

lytic preparations, increasing Co contents favor Co in octahedral locations, probably in 3+ oxidation state. In contrast, preparations with low Co content have a larger proportion of *distorted* octahedral Co(II) (as in CoO or $CoMoO_4$). When the cobalt content was increased the arrangement of oxygen atoms in the catalyst approached that of Co_3O_4, i.e., a mixture of distorted tetrahedra and regular octahedra about the metallic atoms (Figs. 4d–4f).

The peak at 3.35–3.45 Å in these preparations was assigned to Co–Co scattering, calibrated by the overlapped Co(t)–Co(t) and Co(o)–Co(o) in Co_3O_4 at 3.38 Å. The Co(o)–Co(o) from a highly distorted octahedral environment, as in CoO, was found to be at a shorter location, 3.0 Å. A possible alternate assignment of this peak is an overlap of Co–Co and Co–Mo scattering, as in $CoMoO_4$. However, in the *RD* of β-Co MoO_4 (*17*) a peak was found at 3.15 Å (Co–Co at 3.07 Å and Co–Mo at 3.19 Å), while the expected longer overlap (Co–Co at 3.38 Å and Co–Mo at 3.58 Å) was not observed. This weakens the argument that the 3.35- to 3.45-Å peak in the catalyst is due to Co–Mo. The low variable intensity bump in the vicinity of 2.8 Å may arise from small variable contributions from Co(o)–Co(o), which are intense in Co_3O_4.

The peak assignments for preparations with atomic ratio Co/Mo greater than unity are unambiguous. Their $\rho_3(R\psi)$ functions (Figs. 4d–4f) are very similar to that of Co_3O_4; even the fourth shell's peak at 5.0 Å is discernible. This is consistent with the UV reflectance data, recorded for these preparations (*4*). However, the *RD* peak intensities are somewhat smaller than those in the reference compound. Except for absolute magnitude, the 12/12 composition (Co/Mo atomic ratio equal to 2) is indistinguishable from Co_3O_4; in 12/18 (Co/Mo ratio = 1.33), the 2.8 Å peak is considerably lower; in 6/6 (ratio = 2) that trend is continued. Since this is a measure of Co(o)–Co(o) scattering it appears that Mo hinders conversion to a well-crystallized Co_3O_4 structure when the Co loading is too low. The third peak is a combination of Co(o)–Co(o), a short Co(t)–Co(t), and a long Co(t)–Co(t), located at 3.38 Å. There are also contributions from Co(o)–O and from Co(t)–O to this peak. The last peak at 5.00 Å is mainly from Co(o)–Co(o). The relative peak areas at larger R are not quite the same in the catalyst preparations as in Co_3O_4. From the relative intensities of the first two peaks one may conclude that the Co (III)/Co(II) ratios in the catalysts are not quite equal to that of Co_3O_4 (Table 1). In the *RD* curves the position of the first peak in these preparations appears at slightly shorter R than does the first peak in Co_3O_4 but the second peak appears at somewhat longer R than in Co_3O_4. This is also indica-

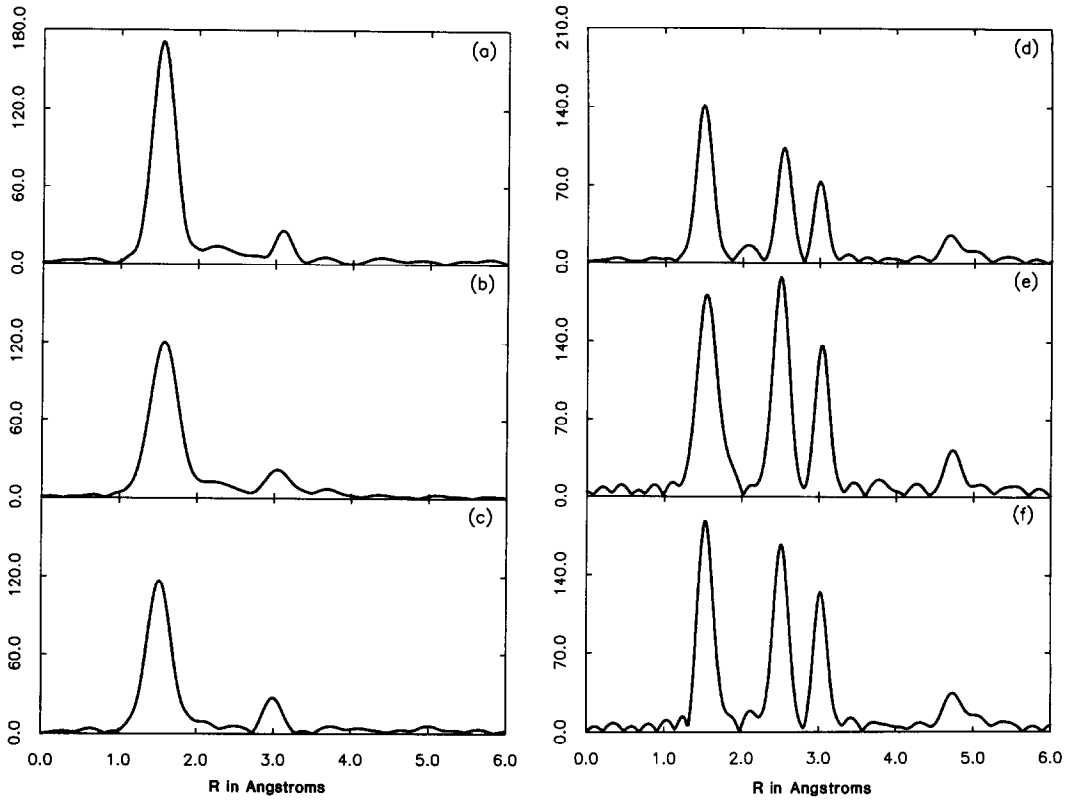

FIG. 4. $\rho_3(R\psi)$ curves of oxide preparations. (a) CoO/MoO_3 = 1.5/12, EXAFS data terminated at k = 11 Å^{-1}; (b) CoO/MoO_3 = 3/12, EXAFS data terminated at k = 11 Å^{-1}; (c) CoO/MoO_3 = 6/12, EXAFS data terminated at k = 11 Å^{-1}; (d) CoO/MoO_3 = 6/6, EXAFS data extended to k = 15 Å^{-1}; (e) CoO/MoO_3 = 12/12, EXAFS data extended to k = 15 Å^{-1}; (f) CoO/MoO_3 = 12/18, EXAFS data extended to k = 15 Å^{-1}.

tive of varying proportions of Co(III) vs (II).

THE SULFIDED STATE

Experimental

The preparative work and the H_2S activity tests were performed at the ARCO Harvey Laboratories. All the oxide samples were reduced by treating them with 10% H_2S/H_2 at atmospheric pressure under a constant flow of about 1 liter/h/g of catalyst, following the 10-h programmed sequence of temperature rises as described in Ref. (*2*). Then the sulfided samples were used for activity tests (Ref. (*3*)) and thus exposed to extended reaction periods in the HDS test reactor. All the treated catalysts were then stored under Ar and sent to Cornell for examination via EXAFS; they were mounted in a glove bag. In addition to this precaution, note that the catalysts were covered with carbon, which provided added protection against possible oxidation. Air oxidation sensitivity tests were previously conducted (*2*) by recording Mo–K edge absorption spectra before and after exposure to the atmosphere for several hours. Intervals of that duration induced no detectable changes in the spectra. It is noted that in bulk MoS_2 is considerably more sensitive to air oxidation than CoS is.

EXAFS and Radial Distributions of the Sulfided HDS Catalyst

Two Fourier transforms of Co_9S_8 EXAFS spectra are shown in Fig. 5. When

TABLE 1

D(*R*) Curves Derived for the Oxide State (Phase-Shift and Scale Corrected)

(Nominal) CoO/MoO_3 (wt%)	Atomic ratio	Peak 1		Peak 2		Peak 3		Peak 4	
		Å	Area	Å	Area	Å	Area	Å	Area
1.5/6	0.49	2.00	384	[a]	[a]	3.31	413	—	—
3./6	0.99	1.96	439	[a]	[a]	3.40	385	—	—
6./6	2.06	1.91	248	2.86	492	3.38	453	5.00	1022
1.5/12	0.24	1.95	469	[a]	[a]	3.49	300	—	—
3./12	0.50	1.97	412	[a]	[a]	3.41	312	—	—
6./12	1.02	1.92	322	[a]	[a]	3.40	294	—	—
12/12	2.17	1.90	442	2.86	1123	3.39	1123	5.02	1626
1.5/18	0.16	2.00	513	[a]	[a]	3.41	313	—	—
3./18	0.33	1.99	453	[a]	[a]	3.40	378	—	—
6./18	0.68	1.96	335	[a]	[a]	3.46	373	—	—
12/18	1.46	1.90	393	2.86	875	3.38	904	5.00	1518
1.5/24	0.12								
3./24	0.25	1.96	409	[a]	[a]	3.41	224	—	—
6./24	0.51								
1.5/30	0.10	2.02	522	[a]	[a]	3.46	302	—	—
3./30	0.20	1.99	492	[a]	[a]	3.36	197	—	—
6./30	0.41								
$Co(AcAc)_3$		1.90	1049	2.76	640				
Co_3O_4		1.92	526	2.86	1665	3.38	1354	5.00	2142
$CoMoO_4$		2.04	512	—	—	3.15	711	—	—

[a] Small peaks present but their intensities are comparable to the noise level.

the extended spectrum (a) was used three peaks were resolved. The first is positioned at 2.19 Å, which is a contribution from two tetrahedral Co(t)–S (at 2.13 and 2.21 Å; phase-shift corrected). The second peak at 2.49 Å is assigned to the combination of Co(o)–S and Co(t)–Co(t) at 2.39 Å. (In Co_9S_8 eight Co atoms occupy tetrahedral sites for every one which is octahedrally surrounded.) The next shell is peaked at 3.51 Å and is assigned to two pairs of Co(t)–Co(t) at 3.48 and 3.54 Å. When the spectrum of Co_9S_8 was truncated at about 11 $Å^{-1}$, only two peaks were resolved (Fig. 5b), and as expected these have wider FWHM. The first peak at 2.37 Å is an overlap of the two at 2.19 and 2.49 Å; the second coincides with the third peak at 3.51 Å. The lesser resolved radial distribution curve (b) proved helpful for analyzing the spectra of the sulfided catalysts, which had to be truncated at 10–12 $Å^{-1}$ because at larger k the presence of minute Ni impurities (possibly from the reactor wall) and general background absorption generated noisy data. Two peaks were found in the transforms of all the preparations, Figs. 5c–5f, except that samples with only 1.5% of CoO, regardless of the molybdenum content, showed only one clearly resolved peak. (A small peak somewhat larger than the noise level wanders over the range 2.9 to 3.4 Å.) There is a trend such that when either Co or Mo content increased, the position of the first peak appeared at larger R, which ranged from 2.0 to 2.2 Å (Table 2). At constant Mo there is a small effect of Co content on the positions of the first peak. However, their positions are clearly *shorter* than the separation of Co(t)–S *in* Co_9S_8, but

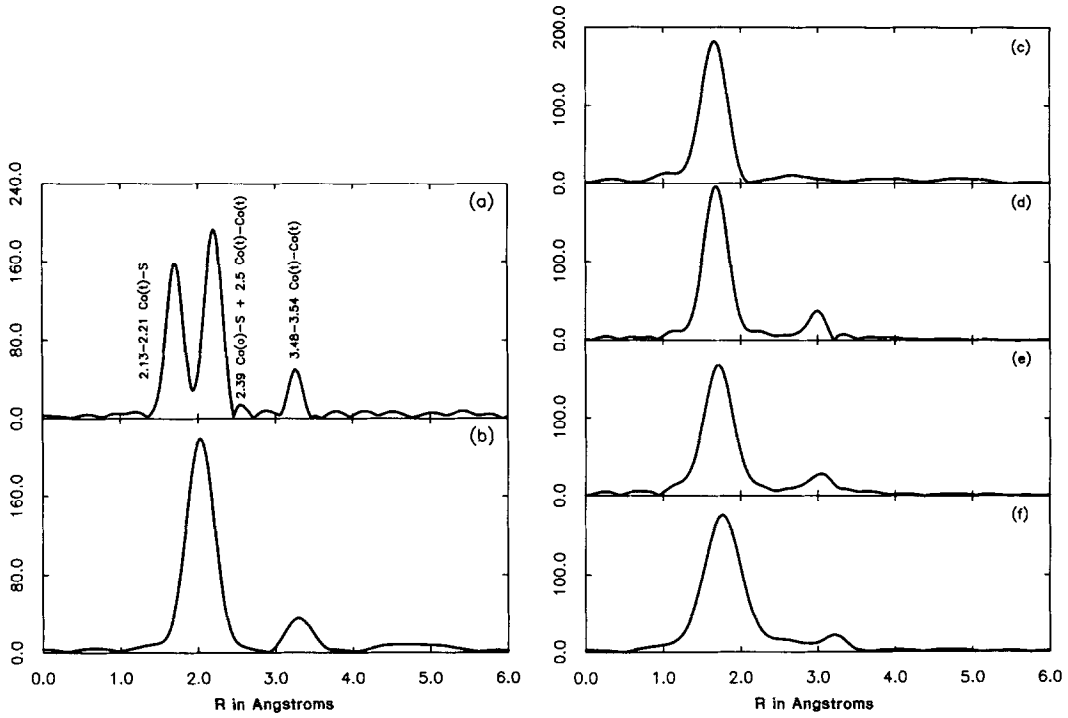

FIG. 5. $\rho_3(R\psi)$ curves for the sulfided and HDS-processed catalysts. (a) Co_9S_8, EXAFS data extended to $k = 15$ Å^{-1}; (b) Co_9S_8, EXAFS data terminated at $k = 12$ Å^{-1}; (c) CoO/MoO_3 (preparations) = 1.5/12, data terminated at $k = 11$ Å^{-1}; (d) CoO/MoO_3 (preparations) = 3.0/12, data terminated at $k = 11$ Å^{-1}; (e) CoO/MoO_3 (preparations) = 6/12, data terminated at $k = 11$ Å^{-1}; (f) CoO/MoO_3 (preparations) = 12/12, data terminated at $k = 11$ Å^{-1}.

are *larger* than Co(o)–O or Co(t)–O separations *in the oxides*. This is a consequence of incomplete sulfiding of the catalysts. When the Co/Mo ratio was increased the first peak moved to longer distances, but it always remained shorter than the first peak in Co_9S_8 (Fig. 5b; per the spectrum terminated at $k = 11$). This indicates that in these preparations more Co–O had been converted to Co–S than in compositions with lower Co/Mo ratios. The lower R value for the first peak could also be due to lesser contributions from Co–Co (2.50 Å in Co_9S_8) because of the amorphous structure of the metal sulfides. The 2.50-Å Co–O peak is only discernible in high cobalt preparations which implies that *segregated Co_9S_8 is present when the cobalt loading is high.* The second peak in the transforms of the sulfided catalysts appears over a relatively wide range, from 3.12 to 3.51 Å. It is possible that this peak is an overlap of the Co–Co in the oxide and the Co–Co in the sulfide (with questionable contributions from Co–Mo).

Due in part to equipment limitations, for the same samples, the EXAFS spectra recorded at the Co–K edge had considerably greater noise than those previously recorded at the Mo–K edge. In addition, previously observed changes in the Mo spectra due to HDS processing, for various Co loadings, suggest that Co tends to diffuse to the platelet peripheries. Presumably, this leads to nonuniform distributions within the platelets, and differing configurations of O, S, and metallic atoms about the Co species. Hence the radial distribution peaks are broad and show insufficient resolution to permit clear assignments to the specific

TABLE 2

D(R) Curves for Sulfided and HDS-Processed Catalysts
(Phase-Shift and Scale Corrected)

(Nominal) CoO/MoO_3 (wt%)	Atomic ratio	Peak 1		Peak 2		Peak 3	
		Å	Area	Å	Area	Å	Area
1.5/6	0.49	1.97	475	—	—	—	—
3./6	0.99	1.96	468	—	—	3.21	303
6./6	2.06	2.16	700	—	—	3.12	329
1.5/12	0.24	1.95	553	—	—	2.98	—
3./12	0.50	2.16	750	—	—	3.12	291
6./12	1.02	2.18	784	—	—	3.14	312
12/12	2.17	2.25	1087	Shoulder		3.42	378
1.5/18	0.16	2.20	773	—	—	—	—
3./18	0.33	2.22	807	—	—	3.15	251
12/18	1.46	2.28	1187	Shoulder		3.50	427
1.5/30	0.10	2.22	897	—	—	—	—
6./30	0.41	2.21	814	—	—	3.14	266
Co_9S_8		2.19	463	2.49	863	3.51	637
Co_9S_8[a]		2.34[a]	1342[a]	—	—	3.51[a]	691[a]
$Co(S_2\text{-}CN\text{-}\varepsilon t_2)_3$		2.26	1543				

[a] When EXAFS spectrum terminated at $k = 11$ Å^{-1}. The catalysts *should be* referenced to these values, to maintain consistency in the data reduction procedure.

atom-pair scattering. Nonetheless, it is possible to partition the magnitudes of the A_1 areas (Table 2) in a rational, although not unique, manner. The collapsed first peak for Co_9S_8, with an area of 1342 units, provides a basis for calibration. Let f_O, f_S, and f_{Co} be the back-scattering coefficients for oxygen, sulfur, and cobalt. From Teo's theoretical tables (*18*), at midrange ($k \approx 8$), the *relative* scattering factors are $f_{Co} \approx 1.69 \cdot f_S$, and $f_O \approx 0.59 \cdot f_S$. Then, from the value for Co_9S_8, for 8-CoS_4 tetrahedra, plus 1-CoS_6 octahedron, plus 3-Co/Co(tet), all in the first coordination shell, one may solve for f_S:

$$1342 = \left[\frac{8 \times 4}{9} + \frac{1 \times 6}{9} + \frac{8 \times 3}{9}(1.69)\right] f_S$$

$$f_S = 153; \quad f_{Co} = 260; \quad f_O = 91.$$

This corresponds to a *mean* (Co–Co) coordination of 2.66, and a *mean* (Co–S) coordination of 4.22. Table 3 shows how the magnitudes of A_1 for these samples can be accounted for, based on the observation that sulfiding is not complete, and its extent increases with Co/Mo loading. The variable (Co–S) coordinations shown are merely residues of the assigned (*Co–O*) and (*Co–Co*) CNs. These values are acceptable indicators of structure but do not show a clear relation to reactivity enhancement. The near-edge profiles show the expected trends with metal loading but no direct correlation with reactivity.

COMMENTS ON RELEVANCE TO CATALYTIC ACTIVITY

We demonstrated (*2, 3*) that the experimental rate constants (κ) correlated with structural parameters derived from *RD* curves, based on EXAFS spectra at the Mo–K edge. The product $\kappa \approx G * Y_S$, where

$$Y_S = \left\{[\text{Mo}]\frac{A(\text{Mo–S})}{2648}\right\}^{1/2},$$

indicates that the major factor responsible for catalytic activity is the number of (Mo–S) atom pairs present at the platelet peripheries, measured by the square root of the area under the (Mo–S) *RD* peak. G was an unspecified Co augmentation factor, assumed constant (47.8). We now propose the *empirical* relation: $G = \varepsilon_1 + \varepsilon_2[\text{Co}]$, where ε_1 measures the low activity of the unpromoted catalyst; ε_2 is the *relative efficiency* per Co, which is high for low loading and declines *smoothly* and *monotonically* with increasing Co concentration, measured as the number of moles per gram of catalyst, per unit area,

$$\varepsilon_2 = \frac{1}{a + b[\text{Co}]^n}. \qquad (1)$$

This is the simplest function which has the observed limiting form. For the 12 preparations prepared for this study, $\varepsilon_1 = 2.70$; $a = 1.807 \times 10^{-8}$; $b = 26.89$; $n = 1.603$. Clearly, high levels of promoter are detrimental; then G approaches an approximate $[\text{Co}]^{-1/2}$ dependence, because the Co_9S_8 phase which is generated covers the peripheries of the platelets (the active sites). The previously computed Y_S values are listed in Table 3, along with the modulated G's and $G * Y_S$. The correlation of κ_{exp} with this product is shown in Fig. 6. This is indeed a better correlation than merely setting G equal to 48.0. For a constant G, the estimated standard deviation is 0.016; it is now reduced to 0.0083.

CONCLUSION

This report completes our studies of 12 specially prepared Mo/Co/alumina hydrodesulfurization catalysts, covering graded sequences in metal loadings on a high area support. Their preparation, physical characterization, reactivity, and X-ray absorp-

TABLE 3

Area and Activity Analysis

Wt% MoO_3	Wt% CoO	Co/Mo atomic ratio	A_1	(Average) partition of A_1 to various atoms			$\kappa_{exp} \times 10^2$	$Y_S \times 10^3$	G_{calc} Eq. (1)	$G * Y_S \times 10^2$
				Co	O	S				
5.9	1.5	0.49	475	0	2	1.91	5.15	1.01	37.0	3.75
5.8	3.0	0.99	468	0	2	1.87	5.16	1.07	52.2	5.59
5.6	6.0	2.06	700	1	1	2.28	4.82	1.02	56.3	5.74
11.8	1.5	0.24	553	0	2	2.42	4.82	1.37	36.7	5.03
11.6	3.0	0.50	750	1	2	2.01	8.20	1.46	51.9	7.59
11.3	6.0	1.02	784	1	1	2.83	9.06	1.51	56.4	8.52
10.6	12.0	2.17	1087	2	1	3.11	6.83	1.52	45.1	6.87
18.0	0	0	0	0	NA	NA	0.5	(1.85)	2.70	(0.50)
17.7	1.5	0.16	773	1	2	2.16	6.68	1.78	37.2	6.63
17.5	3.0	0.33	807	1	2	2.38	9.36	1.85	52.9	9.78
15.8	12.0	1.46	1187	2	1	3.73	8.24	1.82	45.4	8.24
29.6	1.5	0.10	897	1	2	2.97	9.80	2.58	42.3	10.89
28.2	6.0	0.41	814	1	1	3.03	15.92	2.65	53.9	14.27
Co_9S_8			1342	2.66	0	4.22				

Note. Values in ( ) were estimated.

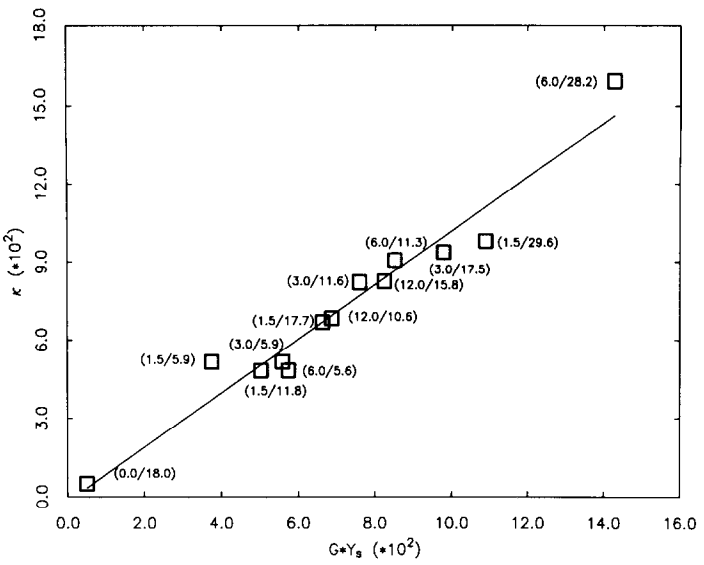

FIG. 6. Correlation between κ_{exp} and $G * Y_S$, computed with $G \equiv \varepsilon_1 + \varepsilon_2[CO]$. The slope of the least-squares line is 1.04.

tion spectra taken at the Mo- and the Co-K edges were carried through in a consistent manner, so that the effects of composition, temperature treatment, and sulfiding would remain under full control. The results of EXAFS and XANES investigations at the Co-K edge compliment those reported previously of the Mo-K edge. From the near-edge profiles we estimated the Co(III)/Co(II) ratio, present in the oxide preparation, and subsequently in the sulfided catalysts. These, as well as the radial distribution curves derived from the extended spectra, indicate that under reactor conditions sulfiding is incomplete, as was demonstrated for the Mo component. When the Co loading was high, a Co_9S_8 phase appeared and thereby reduced the effectiveness of the cobalt as a promoter. Finally, an excellent correlation was established relating the measured catalytic activity rate constant to a product of the square root of the area under the (Mo-S) *RD* peak and the Lorentzian-type function of the Co loading.

ACKNOWLEDGMENTS

This work was supported by a grant from ARCO Petroleum Products Corp., a division of Atlantic Richfield Co. The EXAFS spectra were recorded at the Cornell High Energy Synchrotron Source, supported by NSF Grant DMR-78/267.

REFERENCES

1. Chiu, N. S., Bauer, S. H., and Johnson, M. F. L., *J. Catal.* **89,** 226 (1984).
2. Chiu, N. S., Bauer, S. H., and Johnson, M. F. L., *J. Catal.* **98,** 32 (1986).
3. Johnson, M. F. L., Voss, A. P., Bauer, S. H., and Chiu, N. S., *J. Catal.* **98,** 51 (1986).
4. Recently confirmed by low energy ion scattering spectroscopy; Kasztelan, S., Grimblot, J., and Bonnelle, J. P., *J. Phys. Chem.* **91,** 1503 (1987).
5. Topsøe, H., Clausen, B. S., Topsoe, N.-Y., and Pedersen, E., *Ind. Eng. Chem. Fundam.* **25,** 25 (1986). [A review]
6. Chiu, N.-S., Bauer, S. H., and Johnson, M. F. L., *J. Mol. Struct.* **125,** 33 (1984).
7. Department of Chemistry, University of Minnesota.
8. Bauchspiess, K. R., and Crozier, E. D., "Proceedings of an International Conference, Stanford, CA, July 16–20, 1984" (K. O. Hodgson, B. Hedman, and J. E. Penner-Hahn, Eds.), p. 514. Springer-Verlag, Berlin/New York.
9. (*a*) Stern, E. A., and Heald, S. M., *Rev. Sci. Instrum.* **50,** 1579 (1979); (*b*) Some spectra were collected with the detector borrowed from Dr. Joe Wong of G. E. Research and Development.
10. Bauer, S. H., Chiu, N. S., and Johnson, M. F. L., *J. Phys. Chem.* **90,** 4888 (1986); refer to Note No. 3.

11. Savitzky, A., and Golay, M. J., *Anal. Chem.* **36,** 1627 (1964).

12. Bart, J. C. J., "Advances in Catalysis" (D. D. Eley, P. W. Selwood, and P. B. Weisz, Eds.), Vol. 34, pp. 203–296. Academic Press, San Diego, 1986. [An excellent review]

13. Müller, J. E., Jepsen, O., and Wilkins, J. W., *Solid State Commun.* **42,** 365 (1982).

14. Grunes, L. A., *Phys. Rev. B* **27,** 2111 (1983).

15. Glen, G. L., and Dodd, C. G., *J. Appl. Phys.* **39,** 537 (1968); Tsutsumi, K., Aita, O., and Ichikawa, K., *Phys. Rev. B* **15,** 4638 (1977); Sugiura, C., and Nakai, S.-I., *Japan J. Appl. Phys.* **17**(Suppl. 17-2), 190 (1978).

16. An atomic orbital assignment for Cu^{2+} in $CuCl_2$ was given by Bair, R. A., and Goddard, W. A., III, *Phys. Rev. B* **22,** 2767 (1980).

17. Parham, T. G., and Merrill, R. P., *J. Catal.* **85,** 295 (1984).

18. Teo, B.-K., and Lee, P. A., *J. Amer. Chem. Soc.* **101,** 2815 (1979).